LMO7 regulates smooth muscle cell cholesterol esterification to influence plaque stability

Yi Xie
Yale University
Hanna Winter
Technical University of Munich https://orcid.org/0000-0001-8110-8627
Noemi Rotlan
Yale University
Allison Ostriker
Yale University
Raja Chakraborty
Yale University
Xinbo Zhang
Yale University
John Hwa
Yale University https://orcid.org/0000-0001-7366-2628
Carlos Fernández-Hernando
Yale School of Medicine https://orcid.org/0000-0002-3950-1924
Lars Maegdefessel
Technical University Munich
Kathleen Martin (kathleen.martin@yale.edu)
Yale University https://orcid.org/0000-0002-1748-0034

Article

Keywords:

Posted Date: February 15th, 2022

DOI: https://doi.org/10.21203/rs.3.rs-1359588/v1

Abstract

Smooth muscle cells (SMC) can undergo distinct fate transitions that influence atherosclerotic plaque phenotype: SMC make up the protective fibrous cap that prevents plaque rupture, but can also transdifferentiate to a destabilizing pro-inflammatory phenotype. We found that LMO7, a scaffolding protein that modulates SMC phenotype, is induced in atherosclerosis. SMC LMO7 deletion produced a paradoxical phenotype with enhanced indices of plaque stability despite greater lipid content. We determined that LMO7 promotes SOAT1 ubiquitination and degradation. LMO7 depletion thus favored cholesterol esterification and “safe” storage, relieving ER stress and subsequent induction of KLF4 and SMC transdifferentiation. Immunostaining and single cell sequencing confirmed that SMC LMO7 depletion enhanced cap stabilizing fate transitions while substantially reducing inflammatory transdifferentiation. Similarly, LMO7 was induced in human atherosclerosis, but at lower levels in stable versus ruptured plaques. These findings reveal that SMC cholesterol esterification, rather than total cholesterol content, influences plaque composition and stability.

Introduction

Atherosclerosis is the main cause of morbidity and mortality in the US and Europe. Despite widespread use of lipid lowering agents that help slow the progression, complications of atherosclerotic plaque rupture, including myocardial infarction and stroke, remain major challenges[1]. Accordingly, plaque stability is a key factor in prognosis[2, 3]. New approaches to reduce the incidence of thrombotic events would significantly improve morbidity and mortality consequent to atherosclerosis.

Cholesterol accumulation in the vessel wall leads to plaque formation. Macrophages that engulf the excess cholesterol become foam cells and contribute to a pro-inflammatory milleu[4]. Excessive intracellular cholesterol promotes apoptosis and formation of a necrotic core in the lesions. Smooth muscle cells (SMC) form a protective fibrous cap, providing an essential stabilizing function to separate the pro-thrombotic necrotic core from the lumen[5]. Medial SMC migrate from the plaque shoulder to cover the plaque core at early stages[6]. These SMC secrete copious extracellular matrix (ECM) to form the fibrous cap. Because the thickness and stability of the fibrous cap predicts the vulnerability to rupture[7], SMC are thought to play a protective role in plaques. Recent fate mapping studies have expanded our understanding of the heterogeneity and roles of SMC-derived populations in atherosclerosis. Notably, SMC transdifferentiation to a macrophage-like state is now appreciated to be a major source of foam cells in mouse and human lesions, with 50% of foam cells derived from SMC in human coronary lesions in one analysis[8-10]. The finding that SMC undergo phenotypic modulation to macrophage-like cells in hyperlipidemic conditions[11] suggests a new paradigm where SMC-derived cells can play distinct roles within lesions: the macrophage-like SMC can contribute to the inflammatory lesion core, whereas matrix synthesizing SMC-derived cells act as a protective component in the fibrous cap. Single cell RNA

sequencing (scRNAseq) analyses have demonstrated that SMC can give rise to distinct populations[12] including inflammatory, matrix-producing and osteogenic subtypes[13].

Several studies have recently shown that Kruppel Like Factor 4 (KLF4), a transcription factor implicated in pluripotency, is a key factor promoting SMC dedifferentiation[9, 13, 14]. KLF4 has been shown to play a fundamental role in the SMC phenotypic switching, including in the transition to the pro-inflammatory macrophage-like state[9]. Although expressed in many hematopoietic cells including macrophages, LGALS3 has been identified as a KLF4-regulated marker of phenotypically modulated SMC[13]. LGALS3 expression may represent an early-stage transition that subsequently gives rise to multiple distinct phenotypes during atherosclerosis progression[13]. Early signals through which hypercholesterolemia influences SMC transcription factors and phenotypic switching in atherosclerosis are still poorly understood.

We have recently identified LIM domain only protein 7 (LMO7) as a potent modulator of SMC phenotype[15]. LMO7 is a scaffolding protein containing multiple protein-protein interaction domains. LMO7 loss of function in SMC enhances cell proliferation and ECM deposition following vascular injury[15]. Given the roles for SMC phenotypic modulation, proliferation, and ECM synthesis in atherosclerosis, we hypothesized that LMO7 loss of function may lead to more stable lesions with a thicker fibrous cap.

Methods

Mice. *Lmo7*$^{fl/fl}$ mice on a C57BL/Swiss mixed background were a gift from Dr. Ju Chen (UCSD). *Myh11*-CreER^{T2} and *Apoe*$^{-/-}$ mice were purchased from Jackson Laboratory. Mouse strain with *Gt(ROSA26)-ZsGreen* reporter was a generous gift of Dr. Daniel Greif (Yale). For lineage tracing studies, the *Gt(ROSA26)-ZsGreen* reporter strain was crossed with *Myh11-CreER*^{T2} mice on the *Apoe*$^{-/-}$ background. Recombination was induced by injecting 6 week old mice with 1 mg/kg tamoxifen for 5 days, followed by 5 day washout. Inducible, smooth muscle-specific *Lmo7* knockout mice were generated by crossing the *Lmo7*$^{fl/fl}$ line with the above-mentioned *ROSA26-ZsGreen*/*Myh11-CreER*^{T2}/*Apoe*$^{-/-}$ reporter line. Genotyping of all the mice was performed by PCR. Mice were housed in pathogen-free conditions at Yale University. All experiments were approved by the institutional animal care and use committee of Yale University.

Human tissue studies. Human carotid arteries of the Munich Vascular Biobank[16] were taken during carotid endarterectomy (CEA) followed by fixation for 48 hours in 2% zinc-formalin and paraffin embedding. Per specimen, four 5µm thick sections were stained with hematoxylin and eosin (HE) and Elastin van Gieson's staining. Based on the histochemical stains, plaques were characterized according to

their features as stable or unstable/ruptured following the American Heart Association (AHA) classification after Stary *et al.*[17] and Redgrave *et al.*[18] to determine critical fibrous thickness. Plaque and the non-diseased control portion of the carotid biopsy (as illustrated in Fig. 6a) were separated and lysed for RNA analysis.

Animal experiments. After tamoxifen injection and washout, mice were fed with high fat diet (HFD, 40% kcal%, 1.25% cholesterol, Research Diets D12108C) starting at 8 weeks of age for 0–12 weeks as indicated. For blood lipid assays, mice were starved overnight and anesthetized with 100mg/kg ketamine and 10mg/kg xylazine to collect blood by retro-orbital bleeding before and after HFD feeding. The blood samples were centrifuged at 10,000 rpm for 10 min at R.T. and the plasma (upper phase) was collected for total cholesterol and triglyceride measurement using Cholesterol Assay Kit (Abcam, ab65390) and L-Type Triglyceride M Enzyme Kit (Fujifilm), respectively. Mice were sacrificed at indicated time points post HFD feeding and were immediately perfused first with sodium nitroprusside (SNP) in PBS then 4% paraformaldehyde (PFA). The aortic root (sinus) and the whole aorta as well as brachiocephalic artery (BCA), left common carotid artery, and left subclavian artery branches were dissected and immersed in cold 4% PFA for overnight followed by dehydration in 30% sucrose for another 24 hours. Then the vessels were embedded in OCT compound (Tissue Tek, Elkhart, IN) for cryosectioning.

Mouse single cell RNA sequencing sample preparation and sequencing. After 12 weeks HFD, mice were sacrificed and perfused with PBS. The aortic root, aortic arch and the three major branches, including brachiocephalic artery, left common carotid artery and left subclavian artery were dissected. Tissues were briefly digested in adventitia stripping mix (175U/ml Collagenase II and 1.25U/ml elastase in HBSS) at 37°C for 10 min, and adventitia was peeled off. Then the vessels were cut into 1-2mm long rings and digested in digestion mix (600U/ml collagenase II and 2.5U/ml elastase in HBSS) for 1 h at 37°C with shaking at 700 rpm. Cell suspensions were filtered through 70 μm cell strainer and pelleted at 500 x g for 5 min at 4°C. Cells were then stained in viability staining buffer (0.01 μg/ml DAPI in PBS + 2% FBS) for 5 min at 4°C and maintained in this buffer for cell sorting. DAPI negative Cells were sorted using FACSAria II (BD Biosciences) into DMEM + 10% FBS. Cell numbers were counted and ~ 10,000 cells per sample were used immediately for single-cell library preparation at Yale Keck Biotechnology Resource Laboratory. Cells were loaded into a 10x Genomics microfluidics chip and encapsulated with barcoded oligo-dT-containing gel beads using the 10x Genomics Chromium controller according to the manufacturer's instructions. Single-cell 3' V3.1 libraries were then constructed according to the manufacturer's instructions. Libraries from control and *Lmo7*$^{i\Delta SM}$ samples were multiplexed into one lane and sequenced with setting of paired-end 150bp on an Illumina HiSeq 4000 instrument.

Analysis of scRNASeq data. Fastq files from each mouse genotype were aligned to the reference genome containing *ZsGreen1* gene individually using CellRanger Software (10x Genomics). The dataset was then analyzed using the Partek Flow platform. The dataset was trimmed of cells with read count fewer than 600 or more than 15,000, cells expressing fewer than 500 genes or more than 4,000 genes, and cells with more than 10% mitochondrial counts. The gene expression values then underwent library-size normalization, where raw gene counts from each cell were normalized relative to the total number of read

counts present in that cell. Principal component analysis (PCA) was used for dimensionality reduction, followed by cell clustering using a graph-based clustering approach. t-distributed stochastic neighbor embedding (t-SNE) was then used for two-dimensional visualization of the resulting clusters. Contractile SMC, modulated SMC, fibromyocyte, macrophage, endothelial cell, T cell, neutrophil and fibroblast populations were classified based on the gene expression profile. Cells within the specific classification were combined for further analysis for differential gene expression analysis between control and *Lmo7*$^{i\Delta SM}$ groups.

Histological staining. Haemotoxylin & Eosin (H&E) staining was performed at Yale Pathology Tissue Service using standard protocols. For Picro-Sirius Red (PSR) staining, tissue sections were washed with water to remove OCT and immersed in staining solution (0.1% Direct Red 80 (Sigma, #365548) in a saturated aqueous solution of picric acid) for 1h. The sections were then washed with two changes of 0.5% acetic acid solution, dehydrated with three changes of 100% ethanol, cleared with Histoclear (National Diagnostics, HS-200) and mounted with DPX mounting media (Electron Microscopy Sciences). For *en face* Oil Red O (ORO) staining of aortas, the dissected aorta was cut longitudinally and pinned on a silicon plate. The aorta was fixed with 4% PFA for 1h at RT, briefly rinsed with 78% methanol and immersed in the ORO staining solution (0.2% w/v ORO solution in methanol mixed with 1M NaOH at 7:2 ratio) for 1h. Then the aorta was washed with 78% methanol twice and mounted with OCT medium between two microscope slides. Tissue sections and cell ORO staining follows the same protocol as above. Micrographs of ORO staining was taken with a Nikon Eclipse 80i microscope using NIS Elements software. For filipin staining, cells were washed with PBS and fixed with 4% paraformaldehyde for 1 h at home temperature, followed by incubation with 1.5 mg/ml glycine in PBS for 10 min at room temperature (R.T) to quench the paraformaldehyde. Cells were then stained with filipin working solution (0.05 mg/ml filipin (Sigma, F-9765) in PBS + 10% FBS) for 2 hrs at R.T. Cells were rinsed with PBS twice and were imaged on a Nikon Eclipse Ti Confocal Microscope.

Immunohistochemistry and immunofluorescence. For Immunohistochemistry, cryosections were air-dried completely and fixed/permeabilized in cold acetone for 10 min. OCT was removed by distilled H_2O washing. For TGF-β (MAB1835, clone #1D11, R&D Systems, 1: 25), staining was performed using Mouse-on-Mouse (M.O.M.™, BMK-2202, Vector Laboratories) kit and developed using DAB kit (SK-4100, Vector Laboratories) per manufacturer's protocol. For Ter-119 (14-5921-81, Invitrogen, 1: 100), staining was performed using goat anti-rat HRP (31470, Invitrogen, 1: 500) and developed using DAB kit, followed by Methyl Green counterstain. The sections were mounted in DPX mounting media (Electron Microscopy Sciences) and imaged on a Nikon Eclipse 80i microscope using NIS Elements software. For Immunofluorescence, cryosections were air-dried completely and washed with distilled H_2O to remove OCT. The sections were then permeabilized/blocked in blocking buffer (4% goat normal serum, 1% BSA and 0.5% Triton X-100 in PBS) at room temperature (R.T.) for 1 hr, incubated with primary antibodies at 4°C for 20 hrs, and secondary antibodies at R.T. for 1 hr in blocking buffer. Finally, the sections were stained with DAPI for nuclei at R.T. for 5 min and mounted with Vectashield Mounting Media (Vector Laboratories). The following primary antibodies were used: LMO7 (sc-98422x, Santa Cruz, 1: 100),

LGALS3 (CL8942AP, Cedarlane, 1: 100), ACTA2 (sc-32251 AF546, Alexa 546-conjucated, Santa Cruz, 1: 300), CD68 (MCA1957, Bio-Rad, 1: 100), Ki67 (MA5-14520, Thermo, 1: 200), KLF4 (#4038, Cell Signaling, 1: 100), p-SMAD3 (S423/425) (ab52903, Abcam, 1: 100), ATF4 (#11815, Cell Signaling, 1: 100), SOAT1 (ab39327, Abcam, 1: 100). Appropriate fluorescent secondary antibodies were purchased from Molecular Probes and diluted 1: 300 in blocking buffer. For cleaved Caspase 3 (cCasp3) staining (#9664, Cell Signaling, 1: 150), VECTASTAIN® Elite ABC kit (PK-6101, Vector Laboratories) was used and developed by Tyramide signal amplification (NEL705A001KT, Akoya Biosciences) steps. Micrographs were captured on a Nikon Eclipse Ti Confocal Microscope using Volocity software.

Primary tissue or cell isolation and cell culture. To isolate primary SMC for cell culture mice were sacrificed, perfused with PBS, and the descending aortas were isolated by microdissection. The vessels were briefly digested in adventitia stripping mix (175U/ml Collagenase II and 1.25U/ml elastase in HBSS) for 10 min, and the adventitia was peeled off. Then the vessels were cut into 1-2mm long rings and digested in digestion mix (400U/ml collagenase II, 2.5U/ml elastase and 0.2mg/ml soybean trypsin inhibitor in HBSS) for 1hr at 37°C with shaking at 700rpm. The cell suspension was centrifuged at 20 X g for 5 min, washed once with DMEM + 20% FBS + Penicillin/Streptomycin (Pen/Strep) and plated in culture dish in the same media. Cells were subcultured 1: 3 ~ 4 upon becoming 90% confluent. Primary human aortic SMCs were purchased from Lonza at passage 3 and propagated in M199 media with 10% FBS, 2.7 ng/ml EGF, 2 ng/ml FGF and Pen/Strep (complete media). Cells were used for experiments between passages 4–7. Drugs used in the experiments: Cycloheximide (Sigma, C7698-1G), MG132 (Selleckchem, S2619), methyl-β-cyclodextrin cholesterol (Sigma, C4951), K-604 (Biovision, B-2926).

Transient transfection of siRNA. Transient transfection of small interfering RNA (siRNA) in hCASMC was performed using Lipofectamine® RNAiMAX (Life Technologies). Cells were plated the day before transfection to reach a confluency of 70%. Transfection reagent and siRNA were mixed in OPTI-MEM (Gibco) and added to the cells as per the Lipofectamine instructions. M199 (human ASMC) or DMEM (mouse ASMC) media with 20% FBS was added to the cells after 6 hours. After another 18 hours, the media was changed to M199 complete media (human ASMC) or DMEM + 20% FBS (mouse ASMC). siRNA for LMO7 or SOAT1 and nonsilencing siRNAs (siControl) were purchased from Invitrogen.

Cholesterol biochemical assay. Mouse ASMCs were starved for 16 hrs and treated with 10 ug/ml cholesterol for 72 hrs. Cells were washed with PBS and scraped in 1ml PBS. Cells were spun down at 200 X g for 5 min. 1/10 of the cells were lysed in RIPA buffer and used for protein quantification and the remainder were used for cholesterol assay. Cholesterol was extracted from these cells with 200 ul of chloroform: isopropanol: NP40 (7:11:0.1). The pellet was spun at 15,000xg for 10 min and the supernatant containing lipid was transferred to a clean glass bottle and dried under nitrogen gas. Dried lipid was dissolved with 200 ul 1X Reaction Buffer provided in the Amplex® Red Cholesterol Assay Kit (Invitrogen, A12216). Total cholesterol (TC) was measured using the kit with esterase in the reaction, while free cholesterol (FC) was measured without esterase. Cholesterol ester (CE) level was calculated by subtracting FC from TC. The mass of each cholesterol fraction was normalized to the mass of protein of the corresponding sample.

Cell lysis and western blotting. Cells were briefly washed with PBS and scraped in cold 1X RIPA buffer supplemented with Protease inhibitor cocktail and PhosSTOP (Roche) on ice. Cell lysates were centrifuged at 20,000 x g for 3 min at 4°C and the supernatant was mixed with loading buffer and heated at 95°C for 5 min. Equal amounts of protein from different samples were separated on SDS-PAGE gel, transferred onto PVDF membrane and immunoblotted with primary antibodies at 4°C for 16 hrs and secondary antibodies (Pierce) at R.T. for 1 h. Blots were developed using SuperSignal® Chemiluminescence Substrate (Pierce). Digital images were taken with Gel Doc™ XR + System using ImageLab software. Primary antibodies used: LMO7 for human samples (ab224113, Abcam, 1: 1000), LMO7 for mouse samples (sc-98422x, Santa Cruz, 1: 2000), LGALS3 (CL8942AP, Cedarlane, 1: 1000), MYH11 (M7786, Sigma, 1:1000), KLF4 (ab129473, Abcam, 1: 1000), ATF4 (#11815, Cell Signaling, 1: 1000), CHOP (#2895, Cell Signaling, 1: 500), SOAT1 (ab39327, Abcam, 1: 1000), Ubiquitin (13724, Cayman, 1: 1000), β-Tubulin (sc-9104, Santa Cruz, 1: 500), GAPDH (#2118, Cell Signaling, 1: 2000), β-actin (#3700, Cell Signaling, 1: 1000). Secondary antibodies conjugated with HRP were purchased from Thermo Fisher and used at 1: 3000 dilution. Densitometry of bands was quantitated using ImageJ.

Immunoprecipitation. Cells were washed and scraped as above except using 1X Cell Lysis Buffer (Cell Signaling). After centrifugation, equal amount of cell lysate from each sample was mixed with primary antibodies with gentle rotation at 4°C for 16 hrs. Then magnetic beads (Bio-Rad) were added and rotated for another 2 hrs to pull down antibody-protein complexes. Beads were washed with Cell Lysis Buffer twice and heated in the presence of loading buffer at 95°C for 5 min. Primary antibodies used for IP: SOAT1 (ab39327, Abcam, 1: 100), normal Rabbit IgG (#2729, Cell Signaling). Western analysis was the same as above.

qRT-PCR. Cells were briefly washed with PBS and scraped in TRIzol™ (Invitrogen) and RNA was extracted and purified using Direct-zol™ RNA Miniprep Plus kit (ZYMO Research). cDNA was reverse transcribed using 5X All-In-One RT MasterMix (G486, ABM) with equal amount of RNA from each sample. cDNA was then diluted 1: 10 and used for quantitative real-time PCR analysis (Bio-Rad CFX96 Real-Time System) using BrightGreen qPCR MasterMix (MasterMix-S, ABM). For miRNA analysis, miRNAs were purified using miRNeasy Kit (217004, Qiagen) and reverse transcribed using miRNA cDNA Synthesis Kit (G902, ABM), followed by real-time qPCR analysis using BrightGreen miRNA qPCR MasterMix (MasterMix-mS, ABM). qPCR was analyzed using the delta delta CT method. All samples were run in duplicate, and signals were normalized to the indicated housekeeping genes/microRNAs.

Statistical analysis. Values are presented as mean ± standard error of the mean (SEM). Statistical analysis was performed using Graph-Pad (Prism7). Comparisons between two samples were performed using the nonparametric Mann-Whitney U test. Data sets with three or more groups were analyzed by 2-way ANOVA followed by Holm-Sidak multiple comparisons testing. Comparisons between two curves were performed by Nonlinear Regression with Extra sum-of-squares F test. P-value smaller than 0.05 was considered significant.

Results

LMO7 is induced in mouse atherosclerosis

We examined LMO7 expression in SMC and other cells during murine atherosclerosis development. We generated a smooth muscle-specific, tamoxifen-inducible, ZsGreen reporter mouse in the *Apoe*$^{-/-}$ background (*Myh11_CreER*^{T2}; *Gt(ROSA26)-ZsGreen; Apoe*$^{-/-}$). Tamoxifen treatment results in fluorescent labeling of SMCs and their daughter cells (Suppl Fig. 1a). We subjected these mice to high fat diet (HFD) feeding, harvested the brachiocephalic artery (BCA) at multiple time points, and immunostained for LMO7 and LGALS3[13]. LMO7 expression was relatively low prior to HFD feeding but was greatly induced in the plaque by HFD, although not in medial layer (Suppl Fig. 1a). We found that cholesterol loading of cultured SMC was sufficient to induce robust expression of LMO7 *in vitro* (Suppl Fig. 1b). LMO7 staining was found in ZsGreen^{+} and ZsGreen^{-} cells and was most prominent after 4-weeks HFD feeding in ZsGreen^{-}/LGALS3^{+} cells, which are likely macrophages. However, from 8 weeks onward, there was extensive LMO7 staining in ZsGreen^{+} cells, suggesting potential roles in SMC as well as in macrophages. Intriguingly, LGALS3 staining directly correlated with the LMO7 staining pattern in ZsGreen^{+} cells, suggesting a potential role for LMO7 in transdifferentiating SMC (Suppl Fig. 1a, arrows).

Global Knockout of LMO7 induces larger plaque but with a stabilized structure

To investigate the function of LMO7 during atherosclerosis progression, we compared *Lmo7* global knockout mice (*Lmo7*$^{-/-}$) crossed with *Apoe*$^{-/-}$ mice to *Apoe*$^{-/-}$ control after 12 weeks HFD. There was no significant difference in total plasma cholesterol or triglycerides before and after HFD feeding between the two groups (Suppl Fig. 2a). We observed a significantly larger Oil Red-O (ORO) positive area in the whole aorta *en face*, in segments of the aortic arch, and in the brachiocephalic artery (BCA) in the *Lmo7*$^{-/-}$ mice compared to the controls (Suppl Fig. 2b-c).

We further examined the histological structure of BCA plaques. Lesion size was larger in the *Lmo7*$^{-/-}$ mice, but the necrotic core was smaller, and fibrous cap was thicker (Suppl Fig. 2d), suggesting that LMO7 deletion enhanced plaque stability. We also note a reduced fraction of *Lmo7*$^{-/-}$ mice with erythrocyte infiltration in the plaque (Ter-119 staining), a surrogate for spontaneous plaque rupture (Suppl Fig. 2e). Consistent with this, we observed a larger collagen^{+} area in the *Lmo7*$^{-/-}$ BCA plaques using polarized microscopy of Picro-Sirius Red (PSR) stained sections (Suppl Fig. 2f). These data reveal that global LMO7 knockout yielded a larger but more stabilized plaque.

Knockout of LMO7 in SMC alters SMC phenotype and promotes features of plaque stability

To investigate the function of LMO7 specifically in SMC during atherosclerosis progression, we generated *Gt(ROSA26)-ZsGreen, Lmo7*$^{fl/fl}$*, Myh11_creER*^{T2}*, Apoe*$^{-/-}$ (*Lmo7*$^{i\Delta SM}$) mice. These mice, along with *Gt(ROSA26)-ZsGreen, Lmo7*$^{+/+}$*, Myh11_creER*^{T2}*, Apoe*$^{-/-}$ (control) mice, were injected with tamoxifen and fed with HFD for 12 weeks. There was no significant difference in total cholesterol or triglycerides between the two groups (Fig. 1a). There was no difference in ORO staining in the whole aorta *en face* between the *Lmo7*$^{i\Delta SM}$ and control mice, but we observed a significantly larger ORO positive area in

the aortic arch and BCA plaques in the *Lmo7*$^{i\Delta SM}$ mice (Fig. 1b-c). H&E staining in BCA plaques showed no difference in lesion size between the *Lmo7*$^{i\Delta SM}$ and control mice; however, we noted multiple features of enhanced stability in the *Lmo7*$^{i\Delta SM}$ mice, including a smaller necrotic core and thicker fibrous cap (Fig. 1d), lower fraction of mice with Ter-119^{+} staining (Fig. 1e), and a larger collagen^{+} area (Fig. 1f).

Cell composition is an important determinant of plaque stability[19, 20], with a greater SMC to macrophage ratio in the lesion, and especially in the fibrous cap area, correlating with plaque stability[21]. We observed a larger ACTA2^{+} (SMC) area and smaller CD68^{+} (macrophage) area in the plaques of *Lmo7*$^{i\Delta SM}$ mice compared to controls, and a higher percentage of ACTA2^{+} cells and a lower percentage of CD68^{+} cells in the fibrous cap area of *Lmo7*$^{i\Delta SM}$ mice (Fig. 1g), indicating a more favorable cellular composition.

We noticed a marked increase in SMC-derived (ZsGreen^{+}) cells in the BCA lesions of *Lmo7*$^{i\Delta SM}$ mice compared to controls (Fig. 1g, 2a). To quantitatively assess the phenotypes of these SMC-derived cells, we immunostained for ACTA2 and LGALS3. Similar to CD68 (Fig. 1g), there was a reduction in LGALS3^{+} cells in the *Lmo7*$^{i\Delta SM}$ compared to controls (Fig. 2a). In the fibrous cap, we noted more ZsGreen^{+} cells in *Lmo7*$^{i\Delta SM}$ versus control lesions, and a higher percentage of these cells were ACTA2^{+} (Fig. 2a). There was also a trend toward a lower percentage of ZsGreen^{+} LGALS3^{+} cells relative to total DAPI^{+} nuclei in the cap (Fig. 2a). In the ZsGreen^{+} population, there were more ACTA2^{+} and fewer LGALS3^{+} cells, indicating that the phenotypic modulation of SMC was skewed toward more protective and less inflammatory states in the *Lmo7*$^{i\Delta SM}$ mice. Moreover, the percentage of ZsGreen^{-} LGALS3^{+} cells relative to DAPI^{+} nuclei was also reduced (Fig. 2a), indicating that the recruitment, or retention of macrophages in the lesion was also suppressed in the *Lmo7*$^{i\Delta SM}$ mice.

To determine whether the increased number of SMC-derived (ZsGreen^{+}) cells in the *Lmo7*$^{i\Delta SM}$ lesions was due to altered SMC proliferation and/or apoptosis, we immunostained for Ki67, a proliferation marker, and cleaved caspase 3 (cCasp3), an apoptosis marker, in the BCAs. There were more ZsGreen^{+} Ki67^{+} cells in the fibrous cap of the *Lmo7*$^{i\Delta SM}$ mice (Suppl Fig. 3), indicating enhanced SMC proliferation. This is consistent with our prior report of enhanced SMC proliferation in *Lmo7*$^{i\Delta SM}$ mice following vascular injury[15]. We found that there were fewer ZsGreen^{+} cCasp3^{+} cells within fibrous cap cells (DAPI^{+}) and in the ZsGreen^{+} SMC (Fig. 2b), revealing that LMO7 limits proliferation and promotes apoptosis in plaque SMCs.

Phenotypic modulation by cholesterol treatment is suppressed in LMO7-deficient SMC

We next determined whether LMO7 could regulate cholesterol-induced SMC transdifferentiation *in vitro* by treating primary mouse aortic SMC isolated from WT or *Lmo7*$^{-/-}$ mice with cyclodextrin-balanced cholesterol (as in [11]). As expected, qPCR analysis indicated that cholesterol treatment inhibited *Myh11* and induced *Lgals3* RNA in WT SMC (Fig. 2c). Cholesterol-induced changes in these lineage markers were significantly reduced in *Lmo7*$^{-/-}$ SMC (Fig. 2c), consistent with an inhibited transdifferentiation in the

Lmo7$^{i\Delta SM}$ mice (Fig. 2a). Cholesterol treatment reduces SMC collagen expression *in vitro*[22]. We noted higher RNA levels of several collagen genes in *Lmo7*$^{-/-}$ cells compared to WT both at baseline and after cholesterol treatment (Suppl Fig. 4), consistent with the higher ECM content in the *Lmo7*$^{i\Delta SM}$ mice (Fig. 1f).

We further evaluated KLF4, a master regulator of SMC phenotypic modulation[9]. Similar to *Lgals3*, cholesterol treatment induced *Klf4* mRNA in both WT and *Lmo7*$^{-/-}$ SMC, but to a lesser extent in the *Lmo7*$^{-/-}$ cells (Fig. 2d). These differences were also observed in the protein levels of KLF4, LGALS3 and MYH11 in WT and *Lmo7*$^{-/-}$ SMC lysates (Fig. 2f). Immunostaining for KLF4 was also reduced in BCA lesions in the *Lmo7*$^{i\Delta SM}$ mice (Fig. 2e). Collectively, these data indicate that LMO7 is required for optimal KLF4 expression and SMC phenotypic modulation in response to cholesterol.

LMO7 regulates lineage markers and KLF4 expression via TGF-β-miR-145 axis

Our previous findings demonstrated that loss of LMO7 in SMC induces stronger TGF-β signaling in vascular injury models[15]. Here, in atherosclerosis, we also observed stronger immunostaining for TGF-β as well as p-SMAD3, the major signal-transducer of this pathway, in BCAs of *Lmo7*$^{i\Delta SM}$ mice compared to WT lesions (Suppl Fig. 5a, b). Considering the protective role of the TGF-β pathway in SMC in atherosclerosis[23], we tested whether TGF-β contributes to the anti-transdifferentiation effect of LMO7 depletion. Co-treatment of cultured SMC with cholesterol and SB431542, an inhibitor of TGFβRI, largely eliminated the difference between WT and *Lmo7*$^{-/-}$ in expression of *Myh11, Lgals3,* and *Klf4* (Suppl Fig. 5c).

Previous studies have demonstrated that TGF-β suppresses KLF4 expression by inducing the miR-143/145 microRNA cluster[24]. Moreover, cholesterol treatment induces KLF4 by inhibiting miR-145 in SMC[25]. Therefore, we assessed miR-145 expression in the *Lmo7*$^{-/-}$ SMC after cholesterol and SB431542 treatment. We noticed higher levels of miR-145 at baseline in the *Lmo7*$^{-/-}$ SMC (Suppl Fig. 5d), consistent with increased TGF-β signaling[15]. Cholesterol treatment inhibited miR-145 expression in both WT and *Lmo7*$^{-/-}$ SMC, likely due to the suppression of TGF-β signaling, however, miR-145 expression remained significantly higher in *Lmo7*$^{-/-}$ SMC compared to WT SMC (Suppl Fig. 5d). Lastly, co-treatment of SMC with TGFβRI inhibitor and cholesterol further suppressed miR-145 levels in *Lmo7*$^{-/-}$ SMC down to the expression observed in WT cells (Suppl Fig. 5d). The regulation of miR-145 is consistent with that of KLF4 by LMO7. These data suggest that the TGF-β-miR-145-KLF4 axis could, at least in part, mediate the LMO7-regulated SMC phenotypic modulation.

LMO7 regulates ER stress via cholesterol metabolism

Endoplasmic reticulum (ER) stress is elevated in SMC in hyperlipidemic conditions[26], and has also been implicated in KLF4 regulation: ER stress activates ATF4, which in turn transactivates the *KLF4* gene and inhibits KLF4 protein degradation[27]. We therefore hypothesized that LMO7 may influence KLF4

expression by modifying cholesterol-induced ER stress. Cholesterol treatment induced a significant upregulation of ATF4 and its downstream pro-apoptotic gene CHOP in WT SMC, but not in the *Lmo7*$^{-/-}$ SMC (Fig. 3a). Additionally, immunostaining showed less ATF4 expression in the *Lmo7*$^{i\Delta SM}$ mice compared to control (Fig. 3b), indicating attenuated ER stress.

Excess of free cholesterol (FC) is a major inducer of ER stress[26, 28]. We determined that FC levels as measured by filipin staining were lower in the *Lmo7*$^{-/-}$ SMCs compared to WT cells following cholesterol treatment (Fig. 3c). Differential cholesterol uptake does not likely explain this difference in FC as our cell-based transdifferentiation assays employ a water-soluble cholesterol formulation. Furthermore, there was no difference in *Lrp1* mRNA, the major receptor for LDL uptake in SMC[29] between WT and *Lmo7*$^{-/-}$ SMC (Suppl Fig. 6a). We also found no differences in mRNA for critical genes in the cholesterol biosynthesis pathway, including *Sqle, Cyp51*, *Dhcr24* and *Hmgcr*[30] between WT and *Lmo7*$^{-/-}$ SMC either at baseline or with cholesterol (Suppl Fig. 6b). There was also no change in ABCA1, the main membrane transporter which mediates cholesterol efflux[31] (Suppl Fig. 6c).

We hypothesized that FC was reduced in *Lmo7*$^{-/-}$ SMC through enhanced conversion of FC to cholesterol ester (CE), an important mechanism shown to reduce cholesterol cytotoxicity[26, 32]. This could potentially explain the *in vivo* data showing higher ORO positive area in the aortic arch (Fig. 1b) and BCA (Fig. 1c) of *Lmo7*$^{i\Delta SM}$ mice, as ORO stains specifically neutral lipids including CE but not FC. We performed ORO staining on cholesterol-treated mouse SMC in culture and observed more ORO^{+} lipid droplets in the *Lmo7*$^{-/-}$ SMC (Fig. 3d). This observation correlated with increased cholesterol esters found in LMO7-deficient SMC (Fig. 3e). Total cholesterol (TC) was similar in WT and *Lmo7*$^{-/-}$ SMC but FC reduced in cells lacking Lmo7 (Fig. 3e). Together, these data suggested that the reduced level of FC in *Lmo7*$^{-/-}$ SMC is likely due to its accelerated conversion to CE.

LMO7 regulates SOAT1 expression by mediating its ubiquitination and proteasomal degradation

Sterol o-acyltransferase (SOAT; also called ACAT) catalyzes the conversion of FC to CE. Notably, we observed an increase expression of SOAT1, the major SOAT isoform in SMC, in *Lmo7*$^{-/-}$ SMC compared to WT SMC (Fig. 4a). Concordantly, *in vivo* analysis showed stronger SOAT1 immunofluorescence in ZsGreen^{+} cells in the BCA of the *Lmo7*$^{i\Delta SM}$ mice (Fig. 4b), suggesting that LMO7 may attenuate SOAT1 expression. We did not see a significant difference in *Soat1* mRNA between WT and *Lmo7*$^{-/-}$ SMC (Suppl Fig. 6d), suggesting that LMO7 might control SOAT1 expression at the post-transcriptional level. Thus, we analyzed whether LMO7, an F-box protein that mediates proteasomal degradation of target proteins[15], interacts directly with SOAT1. Our results show that SOAT1 and LMO7 co-immunoprecipitate (Fig. 4c) and suppression of protein synthesis using cycloheximide (CHX) revealed a slower rate of SOAT1 protein decay (enhanced protein half-life) in the *Lmo7*$^{-/-}$ SMC compared to WT cells (Fig. 4d). These results suggest that LMO7 might regulate SOAT1 protein stability and degradation. Indeed, we observed that the proteasome inhibitor MG-132 enhanced the SOAT1 ubiquitin signal in control but not LMO7 depleted cells (Fig. 4e), indicating that LMO7 can mediate the ubiquitination of SOAT1 protein.

To verify the function of SOAT1 in LMO7-mediated SMC phenotypic modulation, we next assessed cholesterol-induced SMC transdifferentiation in the presence of the SOAT1 inhibitor K-604. In both WT and *Lmo7*$^{-/-}$ SMC, SOAT1 inhibition enhanced the induction of KLF4, LGALS3, and the ER stress markers ATF4 and CHOP (Fig. 4f). Importantly, SOAT1 inhibition abrogated the effect of *Lmo7*$^{-/-}$, such that levels of KLF4 and LGALS3 were comparable to WT controls (Fig. 4f). These data suggest that modulation of cholesterol-induced SMC transdifferentiation, by LMO7, requires SOAT1-dependent regulation of cholesterol metabolism.

Single cell RNA sequencing revealed a distinct cellular composition of SMC-derived cells in the *Lmo7*$^{i\Delta SM}$ mice

To comprehensively investigate the changes in plaque composition and SMC phenotype with loss of LMO7, we performed single cell RNA sequencing (scRNAseq) analysis of cells isolated from aortic root, aortic arch and its three major branches which were harvested from control and *Lmo7*$^{i\Delta SM}$ mice (both on Apoe$^{-/-}$ background) fed a HFD for 12 weeks. We combined cell data points from WT and *Lmo7*$^{i\Delta SM}$ groups for analysis and identified 11 populations by graph-based clustering (Fig. 5a). Based on the gene expression profile, we identified all the major cell types in the atherosclerotic lesion, including SMCs, fibroblasts, macrophages (including classically activated- “Macrophage 1”, and alternatively activated- “Macrophage 2” clusters), endothelial cells, neutrophils, and T lymphocytes (Fig. 5b). Five SMC-derived ZsGreen+ clusters were identified (Fig. 5b). Based on the published defining markers for various subpopulations[12, 13], they were classified as “SMC” (classical contractile phenotype SMC), cap-stabilizing “Phactr1^{+} SMC”[13], “Transitioning SMC” (*Klf4*$^{+}$ *Lgals3*$^{+}$ *Myh11*^{low}), inflammatory “Macrophage-like cell” (expressing both SMC and macrophage markers) or rupture-protective “Fibromyocyte”[12] (Fig. 5a, defining genes shown in Fig. 5b). Interestingly, WT and *Lmo7*$^{i\Delta SM}$ mice displayed distinct profiles of SMC-derived populations: WT mice contained 52.2% transitioning SMC, while this population was dramatically reduced (8.0%) in *Lmo7*$^{i\Delta SM}$ mice (Fig. 5c). Conversely, there were many more contractile SMC and slightly increased fibromyocytes in *Lmo7*$^{i\Delta SM}$ mice (Fig. 5c). Interestingly, the macrophage1 cluster was also reduced in *Lmo7*$^{i\Delta SM}$ plaques, suggesting reduced inflammation (Fig. 5c). These data were consistent with the plaque characterization based on immunostaining and lineage tracing in Fig. 1-2.

LMO7 is induced in human atherosclerosis and enriched in ruptured lesions

To determine whether these roles of LMO7 may translate to human atherosclerosis, we evaluated LMO7 mRNA levels in human atherosclerotic arteries from patients undergoing carotid endarterectomy. These samples included normal control regions (Fig. 6a). There was an increase in LMO7 mRNA in all atherosclerotic regions (average of 3-fold induction) compared to a non-diseased control segment of the same artery in each patient (Fig. 6b). Additionally, there was 5.7-fold more LMO7 mRNA in ruptured human plaque samples compared to stable plaques (Fig. 6b). These data reveal a positive correlation between SMC LMO7 expression and atherosclerotic plaque vulnerability in patients.

Discussion

The most salient finding of our study is the identification of LMO7 as a key molecule that integrates cellular cholesterol metabolism and SMC transdifferentiation affecting atherosclerotic plaque composition and stability. We demonstrate that cholesterol-induced LMO7 promotes SOAT1 ubiquitination and degradation leading to accumulation of FC. LMO7 depletion stabilizes SOAT1, promoting cholesterol esterification in SMC. This alleviates ER stress-induced induction of KLF4 and inflammatory SMC fate transitions (Fig. 6c). Finally, our study also reveals that enhancing cholesterol esterification dramatically alters SMC phenotypic modulation and promotes features of plaque stability.

The pathogenesis of atherosclerosis involves the actions of multiple cell types. The complex role of SMCs in this disease was underestimated until recently. Previously, SMCs were thought to de-differentiate to a synthetic phenotype and participate in fibrous cap formation. While SMC transitions are indeed necessary for fibrous cap formation[6, 33], recent studies showed that SMC can also transform into a range of diverse phenotypes in lesions, including macrophage-like cells[9, 11], fibromyocytes[12], osteoblasts and chondrocytes[23]. Since these different phenotypic transitions likely exert distinct or even opposite effects with respect to lesion growth and stability, it is crucial to understand the mechanisms controlling cell fate. In the current study, we demonstrated that loss of LMO7 in SMC led to alteration of intracellular cholesterol processing and phenotypic modulation. A comprehensive scRNAseq analysis showed that the "transitioning" SMC state (*Klf4*$^{+}$ *Lgals3*$^{+}$ *Myh11*^{low}) was substantially reduced in the *Lmo7*$^{i\Delta SM}$ mice, consistent with analysis of lesion cell composition by immunostaining. Moreover, the LMO7-deficient SMC-derived cells presented enhanced proliferation and viability and deposited larger amounts of ECM, leading to features of stable plaque.

We demonstrated that LMO7 modulates cholesterol-induced SMC phenotypic switching *in vitro* via regulation of KLF4 and LGALS3 expression, the two key players in this process[9, 13]. We further showed that suppression of KLF4 and LGALS3 expression in *Lmo7*$^{-/-}$ SMC was due to the attenuated ER stress and ATF4 activity. Previous studies showed that unresolved ER stress leads to apoptosis in macrophages and SMCs[26, 32]. ER stress could also induce dramatic phenotypic modulation in SMCs by activating ATF4, thus inducing KLF4 expression[27]. The Milewicz group recently published a study demonstrating that inhibiting the PERK-eIF2α-ATF4 pathway suppresses SMC transition to macrophage-like cells by cholesterol treatment[34]. This study supports our finding that cholesterol-induced ER stress is a critical mediator of adverse SMC phenotypic modulation in atherosclerosis, and approaches to suppress SMC ER stress may have therapeutic utility.

In addition to cholesterol metabolism and ER stress, our data suggest that LMO7 may also regulate KLF4 and LGALS3 expression via TGF-β1 signaling. Our previous study showed that knockout of LMO7 in SMC induced elevated TGF-β1 expression and signaling, contributing to enhanced collagen deposition in injury-induced vascular remodeling[15]. Interestingly, cholesterol treatment could suppress TGF-β1 signaling and downstream effectors[35]. We now report that SMC LMO7 depletion enhances TGF-β1

expression and signaling in atherosclerotic plaques, and that TGF-β1 inhibition blunts the protective effect of LMO7 depletion on cholesterol-induced SMC transdifferentiation *in vitro*. These data indicate that LMO7 can influence KLF4 expression through a TGF-β1-dependent miR-145 axis. It is likely that the ability of LMO7 to regulate both TGF-β1 signaling and cholesterol esterification accounts for the potent effects of this protein on SMC fate transitions in atherosclerosis.

Lmo7 global knockout or only in SMC-derived cells elicited a similar phenotype of smaller necrotic core and thicker fibrous cap, although $Lmo7^{-/-}$ mice had larger lesions compared to control, while the SMC *Lmo7* deficient mice did not, indicating that LMO7 may also play roles in other relevant cell types. For example, TGF-β1-induced endothelial-mesenchymal transitions can contribute to atherosclerosis[36]. Macrophages may also play a role in the phenotype of $Lmo7^{-/-}$ mice. Intriguingly, in our scRNAseq analysis with $Lmo7^{i\Delta SM}$ mice, we observed a dramatic alteration of macrophage subpopulations, indicating that SMC exert a paracrine effect on macrophages, potentially through TGF-β1 signaling, which has been shown to influence macrophage classical versus alternative activation patterns[37, 38]. Our findings suggest that targeting LMO7 specifically in SMC has beneficial effects on lesion composition without enhancing lesion size.

In atherosclerosis, monocyte-derived macrophages were thought to be the major cell type to process excessive cholesterol, which internalize modified lipoproteins and become foam cells. However, recent studies in human and mouse lesions revealed that majority of the foam cells are derived from SMCs[8, 39]. This finding highlights the role of SMC in cholesterol storage and its contribution to the control of lipid content in the plaque. In our study, loss of LMO7 in SMC enhanced the conversion of FC to CE, a critical step of lipid droplet formation in foam cells, and increase in foam cell number is associated with reduced SMC transition to macrophage-like cells, as well as with a more stable plaque. Interestingly, previous studies showed that foamy cells derived from macrophages are less inflammatory than non-foamy cells[40, 41], suggesting that foam cell formation for lipid storage is a protective mechanism in hyperlipidemic disease.

Current treatments targeting atherosclerotic vascular diseases, including statins and anti-PCSK9 antibodies, aim to lower circulating lipid levels. These therapies have proven to be effective, but there are still an estimated 805,000 myocardial infarctions per year, and stroke accounts for > 5% of all deaths in the US[1], indicating that additional approaches are required to prevent the occurrence of atherothrombotic events. Enhancing plaque stability may be a beneficial strategy. In our study, when cholesterol esterification was enhanced via elevated SOAT1 by manipulating LMO7 expression globally, or in a SMC-specific manner, it induced features of stabilized plaque, with smaller necrotic cores and thicker fibrous caps. This change in cholesterol storage did not affect circulating cholesterol and triglyceride or cellular TC levels, indicating that promoting cholesterol storage in the esterified form can by itself enhance lesion stability, or potentially combine with the existing lipid-lowering therapies to further reduce incidence of myocardial infarction and stroke.

Cholesterol esterification is catalyzed by SOAT, which may therefore serve as a potential drug target. SOAT inhibition has been evaluated in mouse atherosclerosis with conflicting results[42–46]. Studies from the Chang lab showed that myeloid-specific knockout of ACAT1/SOAT1 in *Apoe*$^{-/-}$ mice reduced lesional macrophage content and suppressed atherosclerosis progression[45, 46]. Additionally, administration of an ACAT/SOAT inhibitor in *Apoe*$^{-/-}$ mice reduced atherosclerosis[44]. However, Accad et al. reported that global knockout of SOAT1/ACAT1 reduced neutral lipids but resulted in more macrophages in the lesions[42]. Further, Fazio et al. demonstrated that transplantation of ACTA1/SAOT1-deficient bone marrow to the *LDLR*$^{-/-}$ mice exacerbated atherosclerosis[43], suggesting a beneficial role of macrophage SOAT1. Importantly, in patients receiving standard care for secondary prevention, administration of ACAT/SOAT inhibitors elicited less normalized atheroma volume regression compared to placebo group (ATIVATE trial[47]), and increased the incidence of major cardiovascular events in patients with familial hypercholesterolemia (CAPTIVATE trial[48]), indicating a protective role of SOAT activity in human cardiovascular disease. Our results that loss of LMO7 in SMC promoted plaque stability by induction of SOAT1 expression provide additional insights into the beneficial role of SOAT1. This assertion is strengthened by the finding that inhibition of SOAT activity in mouse ASMC enhanced their transition to macrophage-like cells by cholesterol treatment[11] and abolished the protective effect of LMO7 depletion on this process. These findings suggest that SOAT1 in SMCs attenuates the cholesterol-induced SMC phenotypic transitions that destabilize atherosclerotic plaques, such that enhancing SMC SOAT1 activation and cholesterol esterification may be a potential therapeutic strategy.

We report that LMO7 is induced by cholesterol in SMC in plaques, and regulates cholesterol processing, which, in turn, influences SMC phenotypic transitions, plaque composition, and features of stability. Notably, LMO7 is also induced in human atherosclerosis compared to healthy vessel and is expressed at higher levels in ruptured or unstable compared to stable lesions. Interestingly, an LMO7 SNP (rs2273996) has been associated with human coronary artery disease[49]. These studies suggest that LMO7 expression and binding partners and cholesterol esterification specifically in SMC could be of interest for targeting lesion stability.

Declarations

Acknowledgements

This work was supported by grants from the NIH to K.A.M. (R01HL151222, R01HL142090, R01 HL146101), to J.H. (R01HL115247A, R01HL122815), and to CF-H (R35HL135820). Research in L.M.'s laboratories is funded by the Swedish Heart-Lung-Foundation (20210519), the Swedish Research Council (Vetenkapsrådet, 2019-01577), the German Center for Cardiovascular Research (DZHK), the SFB1123 and TRR267 of the German Research Council (DFG), the National Institutes of Health (NIH; 1R011HL150359-01), the Bavarian State Ministry of Health and Care through the research project *DigiMed* Bayern.

Author Contributions

Y.X., K.A.M., C.F.-H., and L.M. designed and analyzed the experiments. Y.X. and K.A.M. wrote the manuscript. Y.X., H.W. and N.R. performed the experiments. All co-authors contributed to analyzing and interpreting data and editing the manuscript.

Competing Interests statement

The authors declare no competing interests.

References

1. Benjamin EJ, Muntner P, Alonso A, Bittencourt MS, Callaway CW, Carson AP, Chamberlain AM, Chang AR, Cheng S, Das SR, Delling FN, Djousse L, Elkind MSV, Ferguson JF, Fornage M, Jordan LC, Khan SS, Kissela BM, Knutson KL, Kwan TW, Lackland DT, Lewis TT, Lichtman JH, Longenecker CT, Loop MS, Lutsey PL, Martin SS, Matsushita K, Moran AE, Mussolino ME, O'Flaherty M, Pandey A, Perak AM, Rosamond WD, Roth GA, Sampson UKA, Satou GM, Schroeder EB, Shah SH, Spartano NL, Stokes A, Tirschwell DL, Tsao CW, Turakhia MP, VanWagner LB, Wilkins JT, Wong SS, Virani SS, American Heart Association Council on E, Prevention Statistics C and Stroke Statistics S. Heart Disease and Stroke Statistics-2019 Update: A Report From the American Heart Association. Circulation. 2019;139:e56-e528.
2. Kolodgie FD, Virmani R, Burke AP, Farb A, Weber DK, Kutys R, Finn AV and Gold HK. Pathologic assessment of the vulnerable human coronary plaque. Heart. 2004;90:1385–91.
3. Ahmadi A, Stone GW, Leipsic J, Shaw LJ, Villines TC, Kern MJ, Hecht H, Erlinge D, Ben-Yehuda O, Maehara A, Arbustini E, Serruys P, Garcia-Garcia HM and Narula J. Prognostic Determinants of Coronary Atherosclerosis in Stable Ischemic Heart Disease: Anatomy, Physiology, or Morphology? Circ Res. 2016;119:317–29.
4. Gimbrone MA, Jr. and Garcia-Cardena G. Endothelial Cell Dysfunction and the Pathobiology of Atherosclerosis. Circ Res. 2016;118:620–36.
5. Basatemur GL, Jorgensen HF, Clarke MCH, Bennett MR and Mallat Z. Vascular smooth muscle cells in atherosclerosis. Nat Rev Cardiol. 2019;16:727–744.
6. Misra A, Feng Z, Chandran RR, Kabir I, Rotllan N, Aryal B, Sheikh AQ, Ding L, Qin L, Fernandez-Hernando C, Tellides G and Greif DM. Integrin beta3 regulates clonality and fate of smooth muscle-derived atherosclerotic plaque cells. Nat Commun. 2018;9:2073.
7. Burke AP, Farb A, Malcom GT, Liang YH, Smialek J and Virmani R. Coronary risk factors and plaque morphology in men with coronary disease who died suddenly. N Engl J Med. 1997;336:1276–82.
8. Allahverdian S, Chehroudi AC, McManus BM, Abraham T and Francis GA. Contribution of intimal smooth muscle cells to cholesterol accumulation and macrophage-like cells in human atherosclerosis. Circulation. 2014;129:1551–9.

9. Shankman LS, Gomez D, Cherepanova OA, Salmon M, Alencar GF, Haskins RM, Swiatlowska P, Newman AA, Greene ES, Straub AC, Isakson B, Randolph GJ and Owens GK. KLF4-dependent phenotypic modulation of smooth muscle cells has a key role in atherosclerotic plaque pathogenesis. Nat Med. 2015;21:628–37.
10. Bennett MR, Sinha S and Owens GK. Vascular Smooth Muscle Cells in Atherosclerosis. Circ Res. 2016;118:692–702.
11. Rong JX, Shapiro M, Trogan E and Fisher EA. Transdifferentiation of mouse aortic smooth muscle cells to a macrophage-like state after cholesterol loading. Proc Natl Acad Sci U S A. 2003;100:13531–6.
12. Wirka RC, Wagh D, Paik DT, Pjanic M, Nguyen T, Miller CL, Kundu R, Nagao M, Coller J, Koyano TK, Fong R, Woo YJ, Liu B, Montgomery SB, Wu JC, Zhu K, Chang R, Alamprese M, Tallquist MD, Kim JB and Quertermous T. Atheroprotective roles of smooth muscle cell phenotypic modulation and the TCF21 disease gene as revealed by single-cell analysis. Nat Med. 2019;25:1280–1289.
13. Alencar GF, Owsiany KM, K S, Sukhavasi K, Mocci G, Nguyen A, Williams CM, Shamsuzzaman S, Mokry M, Henderson CA, Haskins R, Baylis RA, Finn AV, McNamara CA, Zunder ER, Venkata V, Pasterkamp G, Bjorkegren J, Bekiranov S and Owens GK. The Stem Cell Pluripotency Genes Klf4 and Oct4 Regulate Complex SMC Phenotypic Changes Critical in Late-Stage Atherosclerotic Lesion Pathogenesis. Circulation. 2020.
14. Salmon M, Gomez D, Greene E, Shankman L and Owens GK. Cooperative binding of KLF4, pELK-1, and HDAC2 to a G/C repressor element in the SM22alpha promoter mediates transcriptional silencing during SMC phenotypic switching in vivo. Circ Res. 2012;111:685–96.
15. Xie Y, Ostriker AC, Jin Y, Hu H, Sizer AJ, Peng G, Morris AH, Ryu C, Herzog EL, Kyriakides T, Zhao H, Dardik A, Yu J, Hwa J and Martin KA. LMO7 Is a Negative Feedback Regulator of Transforming Growth Factor beta Signaling and Fibrosis. Circulation. 2019;139:679–693.
16. Pelisek J, Hegenloh R, Bauer S, Metschl S, Pauli J, Glukha N, Busch A, Reutersberg B, Kallmayer M, Trenner M, Wendorff H, Tsantilas P, Schmid S, Knappich C, Schaeffer C, Stadlbauer T, Biro G, Wertern U, Meisner F, Stoklasa K, Menges AL, Radu O, Dallmann-Sieber S, Karlas A, Knipfer E, Reeps C, Zimmermann A, Maegdefessel L and Eckstein HH. Biobanking: Objectives, Requirements, and Future Challenges-Experiences from the Munich Vascular Biobank. J Clin Med. 2019;8.
17. Stary HC, Chandler AB, Dinsmore RE, Fuster V, Glagov S, Insull W, Jr., Rosenfeld ME, Schwartz CJ, Wagner WD and Wissler RW. A definition of advanced types of atherosclerotic lesions and a histological classification of atherosclerosis. A report from the Committee on Vascular Lesions of the Council on Arteriosclerosis, American Heart Association. Circulation. 1995;92:1355–74.
18. Redgrave JN, Gallagher P, Lovett JK and Rothwell PM. Critical cap thickness and rupture in symptomatic carotid plaques: the oxford plaque study. Stroke. 2008;39:1722–9.
19. Davies MJ, Richardson PD, Woolf N, Katz DR and Mann J. Risk of thrombosis in human atherosclerotic plaques: role of extracellular lipid, macrophage, and smooth muscle cell content. Br Heart J. 1993;69:377–81.

20. Libby P and Aikawa M. Stabilization of atherosclerotic plaques: new mechanisms and clinical targets. Nat Med. 2002;8:1257–62.
21. Tabas I, Garcia-Cardena G and Owens GK. Recent insights into the cellular biology of atherosclerosis. J Cell Biol. 2015;209:13–22.
22. Frontini MJ, O'Neil C, Sawyez C, Chan BM, Huff MW and Pickering JG. Lipid incorporation inhibits Src-dependent assembly of fibronectin and type I collagen by vascular smooth muscle cells. Circ Res. 2009;104:832–41.
23. Chen PY, Qin L, Li G, Malagon-Lopez J, Wang Z, Bergaya S, Gujja S, Caulk AW, Murtada SI, Zhang X, Zhuang ZW, Rao DA, Wang G, Tobiasova Z, Jiang B, Montgomery RR, Sun L, Sun H, Fisher EA, Gulcher JR, Fernandez-Hernando C, Humphrey JD, Tellides G, Chittenden TW and Simons M. Smooth Muscle Cell Reprogramming in Aortic Aneurysms. Cell Stem Cell. 2020;26:542–557 e11.
24. Davis-Dusenbery BN, Chan MC, Reno KE, Weisman AS, Layne MD, Lagna G and Hata A. down-regulation of Kruppel-like factor-4 (KLF4) by microRNA-143/145 is critical for modulation of vascular smooth muscle cell phenotype by transforming growth factor-beta and bone morphogenetic protein 4. The Journal of biological chemistry. 2011;286:28097–110.
25. Vengrenyuk Y, Nishi H, Long X, Ouimet M, Savji N, Martinez FO, Cassella CP, Moore KJ, Ramsey SA, Miano JM and Fisher EA. Cholesterol loading reprograms the microRNA-143/145-myocardin axis to convert aortic smooth muscle cells to a dysfunctional macrophage-like phenotype. Arterioscler Thromb Vasc Biol. 2015;35:535–46.
26. Kedi X, Ming Y, Yongping W, Yi Y and Xiaoxiang Z. Free cholesterol overloading induced smooth muscle cells death and activated both ER- and mitochondrial-dependent death pathway. Atherosclerosis. 2009;207:123–30.
27. Zhou AX, Wang X, Lin CS, Han J, Yong J, Nadolski MJ, Boren J, Kaufman RJ and Tabas I. C/EBP-Homologous Protein (CHOP) in Vascular Smooth Muscle Cells Regulates Their Proliferation in Aortic Explants and Atherosclerotic Lesions. Circ Res. 2015;116:1736–43.
28. Feng B, Yao PM, Li Y, Devlin CM, Zhang D, Harding HP, Sweeney M, Rong JX, Kuriakose G, Fisher EA, Marks AR, Ron D and Tabas I. The endoplasmic reticulum is the site of cholesterol-induced cytotoxicity in macrophages. Nat Cell Biol. 2003;5:781–92.
29. Llorente-Cortes V, Martinez-Gonzalez J and Badimon L. LDL receptor-related protein mediates uptake of aggregated LDL in human vascular smooth muscle cells. Arterioscler Thromb Vasc Biol. 2000;20:1572–9.
30. Luo J, Yang H and Song BL. Mechanisms and regulation of cholesterol homeostasis. Nat Rev Mol Cell Biol. 2020;21:225–245.
31. Castiglioni S, Monti M, Arnaboldi L, Canavesi M, Ainis Buscherini G, Calabresi L, Corsini A and Bellosta S. ABCA1 and HDL3 are required to modulate smooth muscle cells phenotypic switch after cholesterol loading. Atherosclerosis. 2017;266:8–15.
32. Devries-Seimon T, Li Y, Yao PM, Stone E, Wang Y, Davis RJ, Flavell R and Tabas I. Cholesterol-induced macrophage apoptosis requires ER stress pathways and engagement of the type A scavenger

receptor. J Cell Biol. 2005;171:61–73.

33. Cherepanova OA, Gomez D, Shankman LS, Swiatlowska P, Williams J, Sarmento OF, Alencar GF, Hess DL, Bevard MH, Greene ES, Murgai M, Turner SD, Geng YJ, Bekiranov S, Connelly JJ, Tomilin A and Owens GK. Activation of the pluripotency factor OCT4 in smooth muscle cells is atheroprotective. Nat Med. 2016;22:657–65.
34. Chattopadhyay A, Kwartler CS, Kaw K, Li Y, Kaw A, Chen J, LeMaire SA, Shen YH and Milewicz DM. Cholesterol-Induced Phenotypic Modulation of Smooth Muscle Cells to Macrophage/Fibroblast-like Cells Is Driven by an Unfolded Protein Response. Arterioscler Thromb Vasc Biol. 2020:ATVBAHA120315164.
35. Chen CL, Liu IH, Fliesler SJ, Han X, Huang SS and Huang JS. Cholesterol suppresses cellular TGF-beta responsiveness: implications in atherogenesis. J Cell Sci. 2007;120:3509–21.
36. Chen PY, Qin L, Li G, Wang Z, Dahlman JE, Malagon-Lopez J, Gujja S, Cilfone NA, Kauffman KJ, Sun L, Sun H, Zhang X, Aryal B, Canfran-Duque A, Liu R, Kusters P, Sehgal A, Jiao Y, Anderson DG, Gulcher J, Fernandez-Hernando C, Lutgens E, Schwartz MA, Pober JS, Chittenden TW, Tellides G and Simons M. Endothelial TGF-beta signalling drives vascular inflammation and atherosclerosis. Nat Metab. 2019;1:912–926.
37. Gong D, Shi W, Yi SJ, Chen H, Groffen J and Heisterkamp N. TGFbeta signaling plays a critical role in promoting alternative macrophage activation. BMC Immunol. 2012;13:31.
38. Ostriker A, Horita HN, Poczobutt J, Weiser-Evans MC and Nemenoff RA. Vascular smooth muscle cell-derived transforming growth factor-beta promotes maturation of activated, neointima lesion-like macrophages. Arterioscler Thromb Vasc Biol. 2014;34:877–86.
39. Wang Y, Dubland JA, Allahverdian S, Asonye E, Sahin B, Jaw JE, Sin DD, Seidman MA, Leeper NJ and Francis GA. Smooth Muscle Cells Contribute the Majority of Foam Cells in ApoE (Apolipoprotein E)-Deficient Mouse Atherosclerosis. Arterioscler Thromb Vasc Biol. 2019;39:876–887.
40. Spann NJ, Garmire LX, McDonald JG, Myers DS, Milne SB, Shibata N, Reichart D, Fox JN, Shaked I, Heudobler D, Raetz CR, Wang EW, Kelly SL, Sullards MC, Murphy RC, Merrill AH, Jr., Brown HA, Dennis EA, Li AC, Ley K, Tsimikas S, Fahy E, Subramaniam S, Quehenberger O, Russell DW and Glass CK. Regulated accumulation of desmosterol integrates macrophage lipid metabolism and inflammatory responses. Cell. 2012;151:138–52.
41. Kim K, Shim D, Lee JS, Zaitsev K, Williams JW, Kim KW, Jang MY, Seok Jang H, Yun TJ, Lee SH, Yoon WK, Prat A, Seidah NG, Choi J, Lee SP, Yoon SH, Nam JW, Seong JK, Oh GT, Randolph GJ, Artyomov MN, Cheong C and Choi JH. Transcriptome Analysis Reveals Nonfoamy Rather Than Foamy Plaque Macrophages Are Proinflammatory in Atherosclerotic Murine Models. Circ Res. 2018;123:1127–1142.
42. Accad M, Smith SJ, Newland DL, Sanan DA, King LE, Jr., Linton MF, Fazio S and Farese RV, Jr. Massive xanthomatosis and altered composition of atherosclerotic lesions in hyperlipidemic mice lacking acyl CoA:cholesterol acyltransferase 1. J Clin Invest. 2000;105:711–9.

43. Fazio S, Major AS, Swift LL, Gleaves LA, Accad M, Linton MF and Farese RV, Jr. Increased atherosclerosis in LDL receptor-null mice lacking ACAT1 in macrophages. J Clin Invest. 2001;107:163–71.
44. Kusunoki J, Hansoty DK, Aragane K, Fallon JT, Badimon JJ and Fisher EA. Acyl-CoA:cholesterol acyltransferase inhibition reduces atherosclerosis in apolipoprotein E-deficient mice. Circulation. 2001;103:2604–9.
45. Huang LH, Melton EM, Li H, Sohn P, Rogers MA, Mulligan-Kehoe MJ, Fiering SN, Hickey WF, Chang CC and Chang TY. Myeloid Acyl-CoA:Cholesterol Acyltransferase 1 Deficiency Reduces Lesion Macrophage Content and Suppresses Atherosclerosis Progression. J Biol Chem. 2016;291:6232–44.
46. Melton EM, Li H, Benson J, Sohn P, Huang LH, Song BL, Li BL, Chang CCY and Chang TY. Myeloid Acat1/Soat1 KO attenuates pro-inflammatory responses in macrophages and protects against atherosclerosis in a model of advanced lesions. J Biol Chem. 2019;294:15836–15849.
47. Nissen SE, Tuzcu EM, Brewer HB, Sipahi I, Nicholls SJ, Ganz P, Schoenhagen P, Waters DD, Pepine CJ, Crowe TD, Davidson MH, Deanfield JE, Wisniewski LM, Hanyok JJ, Kassalow LM and Investigators AIATE. Effect of ACAT inhibition on the progression of coronary atherosclerosis. N Engl J Med. 2006;354:1253–63.
48. Meuwese MC, de Groot E, Duivenvoorden R, Trip MD, Ose L, Maritz FJ, Basart DC, Kastelein JJ, Habib R, Davidson MH, Zwinderman AH, Schwocho LR, Stein EA and Investigators C. ACAT inhibition and progression of carotid atherosclerosis in patients with familial hypercholesterolemia: the CAPTIVATE randomized trial. JAMA. 2009;301:1131–9.
49. LeBlanc M, Zuber V, Andreassen BK, Witoelar A, Zeng L, Bettella F, Wang Y, McEvoy LK, Thompson WK, Schork AJ, Reppe S, Barrett-Connor E, Ligthart S, Dehghan A, Gautvik KM, Nelson CP, Schunkert H, Samani NJ, Consortium CA, Ridker PM, Chasman DI, Aukrust P, Djurovic S, Frigessi A, Desikan RS, Dale AM and Andreassen OA. Identifying Novel Gene Variants in Coronary Artery Disease and Shared Genes With Several Cardiovascular Risk Factors. Circ Res. 2016;118:83–94.

Figures

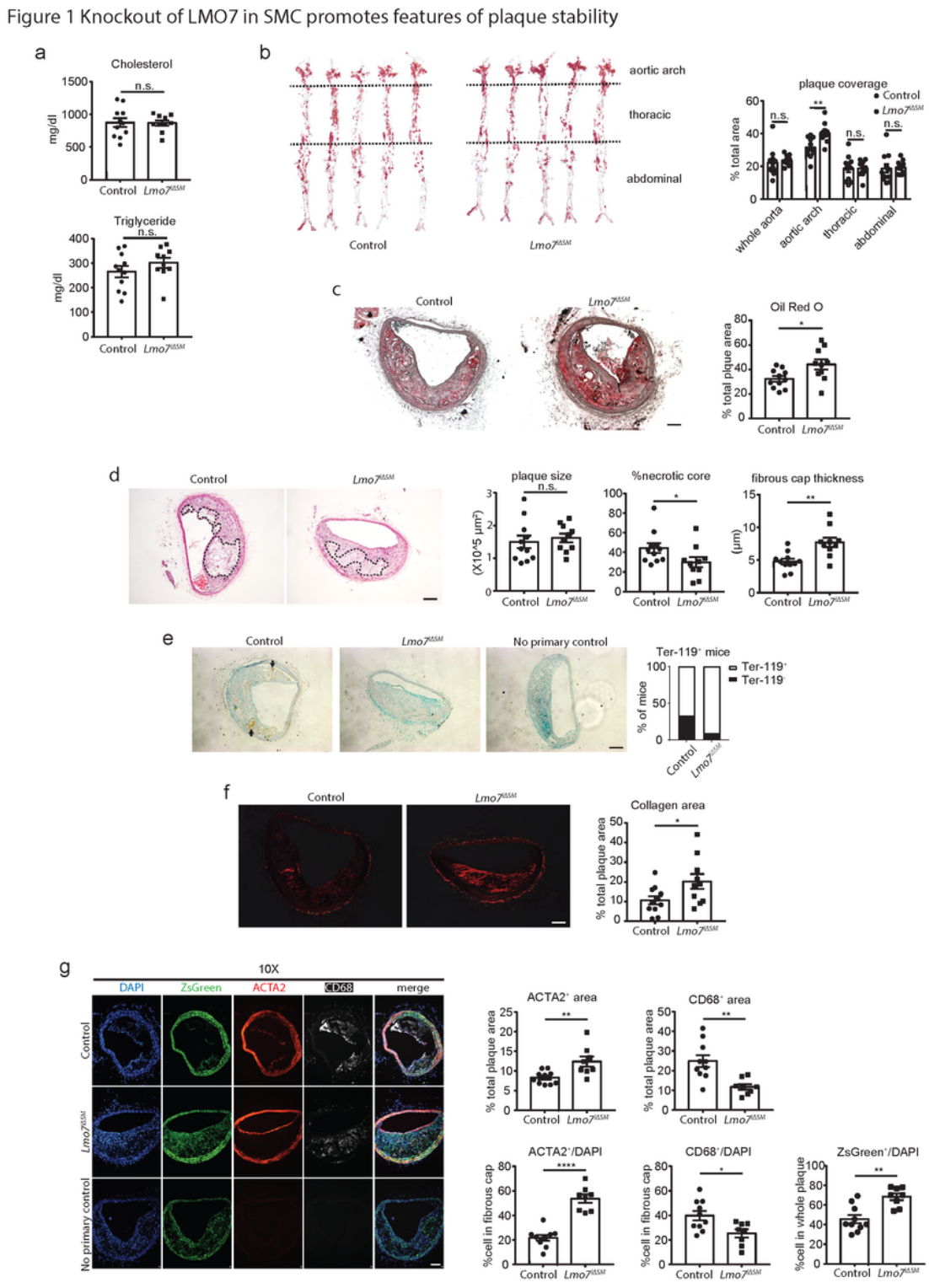

Figure 1

Loss of LMO7 in SMC induces feature of stable plaque in atherosclerosis. *Gt(ROSA26)-ZsGreen, Lmo7$^{fl/fl}$, Myh11_creER^{T2}, Apoe$^{-/-}$ (ZsGreen^{Gt}, Lmo7$^{i\Delta SM}$, Apoe$^{-/-}$)* and *Gt(ROSA26)-ZsGreen, Lmo7$^{+/+}$, Myh11_creER^{T2}, Apoe$^{-/-}$* (control) mice were injected with 1mg/kg tamoxifen at 6-week old for 5 days, followed by washout for 5 days. The mice were then fed with HFD for 12 weeks. (a) The plasma was harvested, and cholesterol and triglyceride levels were measured as shown in the Methods. (b) The aorta

and the three branches of aortic arch were harvested. The BCA was dissected for histological analysis and the rest was subjected to *en face* Oil Red O (ORO) staining. The positive area was quantified using ImageJ in the whole aorta or in the aortic arch, thoracic aorta and abdominal aorta region, separately, and normalized to the whole area of the corresponding region. (c) The cross-sections of BCA were subjected to ORO staining and the positive area was quantified against the whole plaque area. (d) The cross-sections of BCA were subjected to Haematoxylin & Eosin (H&E) staining and the area of plaque and necrotic core and thickness of fibrous cap were quantified using ImageJ. The necrotic core was defined as the area without intact cells and normalized to the whole plaque area. The thickness of fibrous cap was defined as the shortest distance from lumen to the largest necrotic core in the plaque. (e) The cross-sections of BCA were subjected to immunohistochemistry for Ter-119, and counterstained with Methyl Green. The percentage of mice with a positive staining of Ter-119 in the BCA was shown on the right. (f) The cross-sections of BCA were subjected to Picro-Sirius Red (PSR) staining. The positive area was quantified using ImageJ and normalized to the whole plaque area. (n=11 for control, n=10 for $Lmo7^{i\Delta SM}$) (g) The cross-sections of BCA were immunostained for ACTA2 (red) and CD68 (Cy5). $ACTA2^{+}$ and $CD68^{+}$ area was quantified using ImageJ and normalized to the whole plaque area. In the fibrous cap area, $ACTA2^{+}$ and $CD68^{+}$ cells were counted and normalized all fibrous cap cells ($DAPI^{+}$). (n=10 for control, n=7 for $Lmo7^{i\Delta SM}$) Scale bar, 50 μm. Data are expressed as mean±SEM. *P<0.05, **P<0.01, ****P<0.0001.

Figure 2 LMO7 deficiency abrogates SMC phenotypic modulation and apoptosis, but induces proliferation

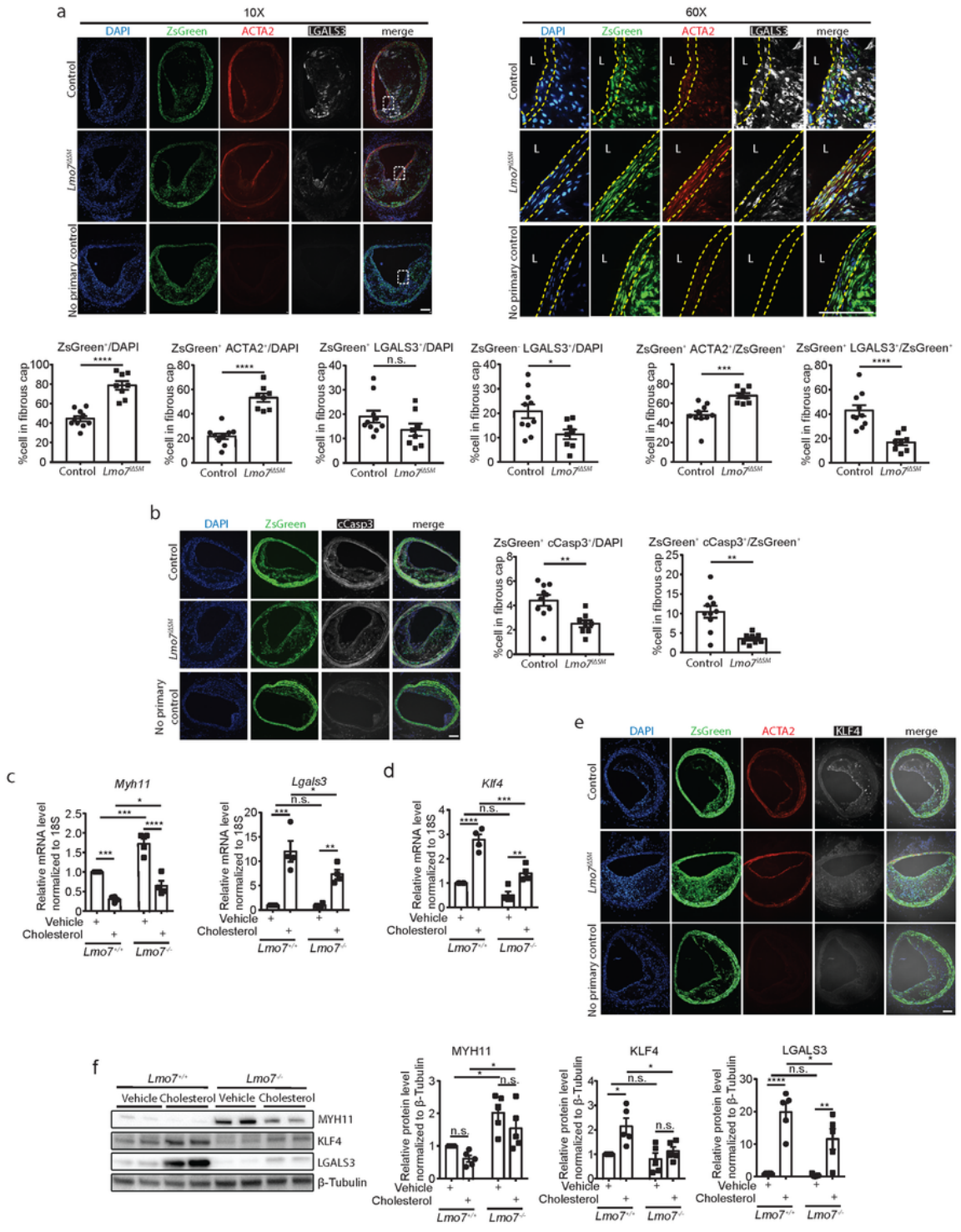

Figure 2

Loss of LMO7 in SMC suppresses phenotypic modulation and promotes cell viability *in vivo*. (a) The cross-sections of BCA were immunostained for ACTA2 (red) and LGALS3 (Cy5). The ZsGreen^{+}, ZsGreen^{+} ACTA2^{+}, ZsGreen^{+} LGALS3^{+}, ZsGreen^{-} LGALS3^{+} cell populations were counted and normalized to all the cells (DAPI^{+}) or ZsGreen^{+} cells in the fibrous cap area as indicated. (b) The cross-sections of BCA were

immunostained for cleaved Caps3 (cCasp3) (Cy5). The ZsGreen^{+} cCasp3^{+} and LGALS3^{+} cCasp3^{+} cell populations were counted and normalized to all the cells (DAPI^{+}) or ZsGreen^{+} cells in the fibrous cap area. (n=10 for control, n=8 for *Lmo7*$^{i\Delta SM}$) (c, d) Mouse aortic SMCs were starved as in the Methods and treated with 40 μg/ml methyl-β-cyclodextrin cholesterol for 72 hrs. The cell lysates were harvested and mRNA was purified for real time qPCR analysis of (c) *Myh11*, *Lgals3* and (d) *Klf4* (n=4). (e) The serial sections as shown in Fig. 1g were immunostained for ACTA2 (red) and KLF4 (Cy5). (f) Mouse ASMCs were starved and treated with cholesterol as in (c, d) and the cell lysates were harvested for western analysis of MYH11, KLF4 and LGALS3, using β-Tubulin as loading control. (n=5) Scale bar, 50 μm. Data are expressed as mean±SEM. **P*<0.05, ***P*<0.01, ****P*<0.001, *****P*<0.0001.

Figure 3 LMO7 regulates ER stress via cholesterol metabolism

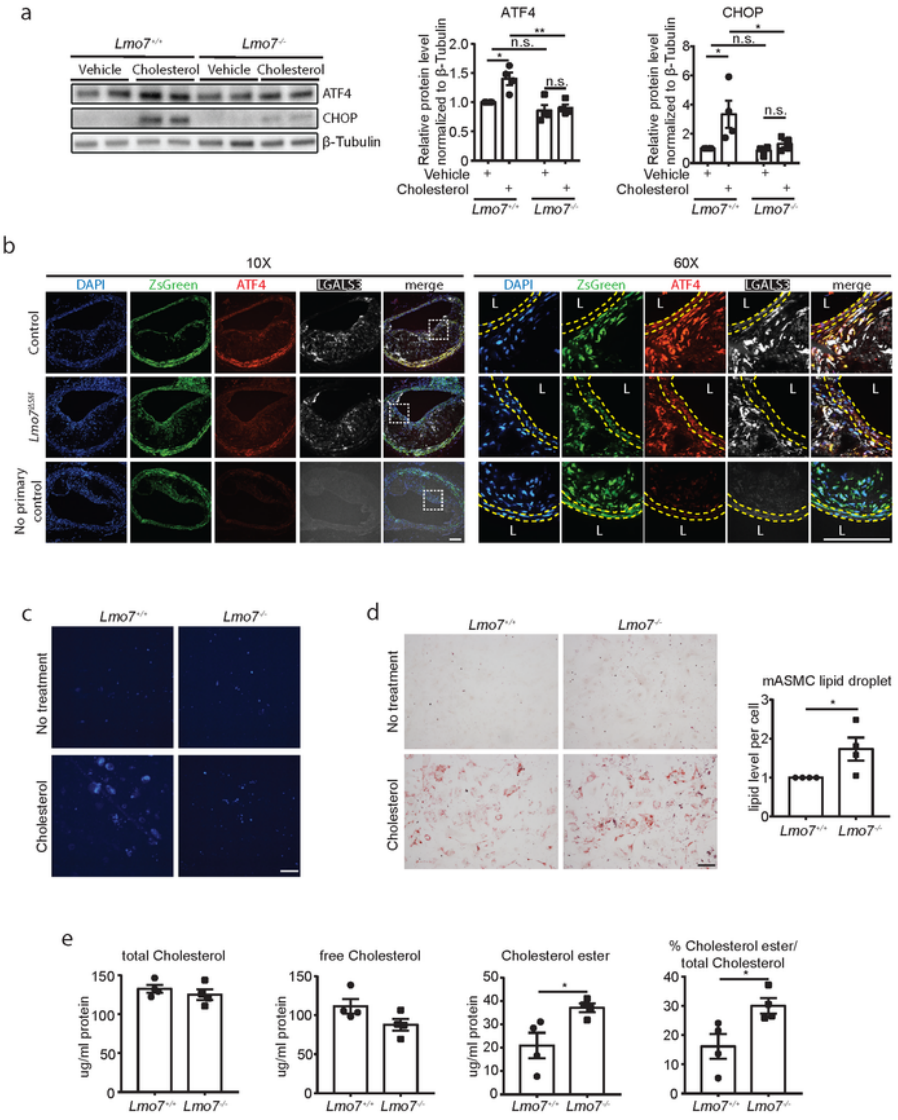

Figure 3

LMO7 regulates ER stress via cholesterol metabolism. (a) Mouse aortic SMCs were starved as in the Methods and treated with 40 μg/ml methyl-β-cyclodextrin cholesterol for 72 hrs, and the cell lysates were harvested for western analysis of ATF4 and CHOP, using β-Tubulin as loading control (n=4). (b) The cross-sections of BCA were immunostained for ATF4 (red) and LGALS3 (Cy5). (c, d) Mouse aortic SMCs were starved as in the Methods and treated with 40 μg/ml methyl-β-cyclodextrin cholesterol for 72 hrs,

and cells were fixed for (c) filipin staining or (d) ORO staining (n=4). (e) Mouse aortic SMCs were starved as in the Methods and treated with 10 μg/ml methyl-β-cyclodextrin cholesterol for 72 hrs. The cells were scrapped in PBS and cholesterol was extracted as shown in the Methods and subjected to analysis using Amplex® Red Cholesterol Kit (n=4). Scale bar, 50 μm. Data are expressed as mean±SEM. *P<0.05, **P<0.01.

Figure 4 LMO7 regulates SOAT1 expression by mediating its ubiquitination and proteasomal degradation

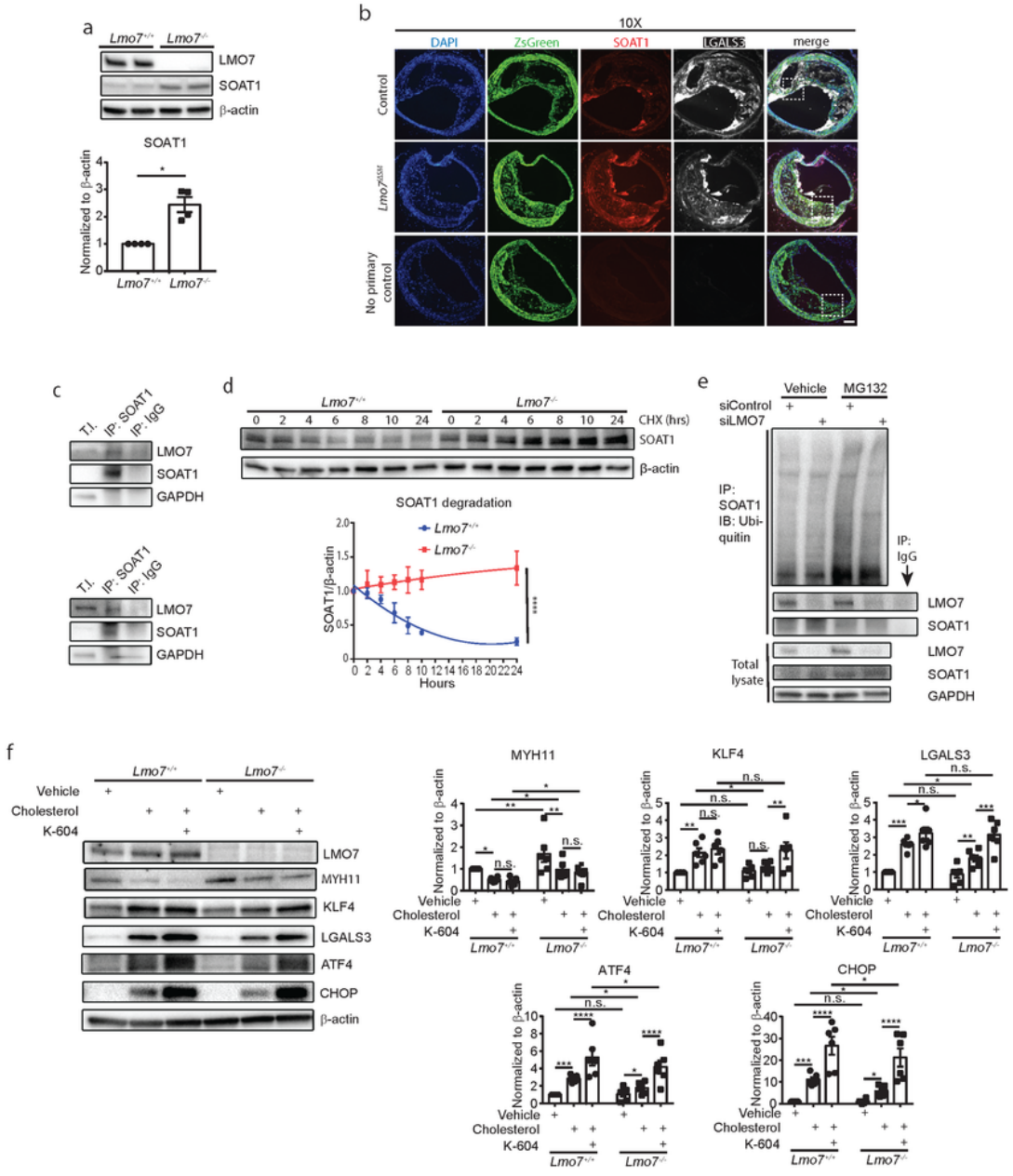

Figure 4

LMO7 regulates SOAT1 expression by mediating its ubiquitination and proteasomal degradation. (a) Mouse aortic SMCs were starved as in the Methods and treated with 40 μg/ml methyl-β-cyclodextrin cholesterol for 72 hrs, and the cell lysates were harvested for western analysis of SOAT1, using β-actin as loading control (n=4). (b) The cross-sections of BCA were immunostained for SOAT1 (red) and LGALS3 (Cy5). (c) Endogenous SOAT1 protein was pulled down by specific antibody and the immunoprecipitates were subjected to western analysis of LMO7 (Representative of 3 biological repeats). (d) mASMCs were starved in 0.5% FBS and treated with Cycloheximide (CHX). Cell lysates were harvested at various time points as indicated and subjected to western analysis for SOAT1, using β-actin as loading control (n=4). (e) Human aortic SMCs were transfected with control siRNA or siRNA for LMO7 for two days, followed by vehicle or MG-132 treatment for another 24 hrs. The cell lysates were harvested for SOAT1 immunoprecipitation and blotted for ubiquitin and LMO7 (n=2). (f) Mouse aortic SMCs were starved for 24 hrs as in the Methods and were treated with 40 μg/ml methyl-β-cyclodextrin cholesterol with or without 10 μM K-604 for 72 hrs, and the cell lysates were harvested for western analysis of various markers as shown, using β-actin as loading control (n=6). Scale bar, 50 μm. Data are expressed as mean±SEM. *P<0.05, **P<0.01, ***P<0.001, ****P<0.0001.

Figure 5 Single cell RNA sequencing analysis

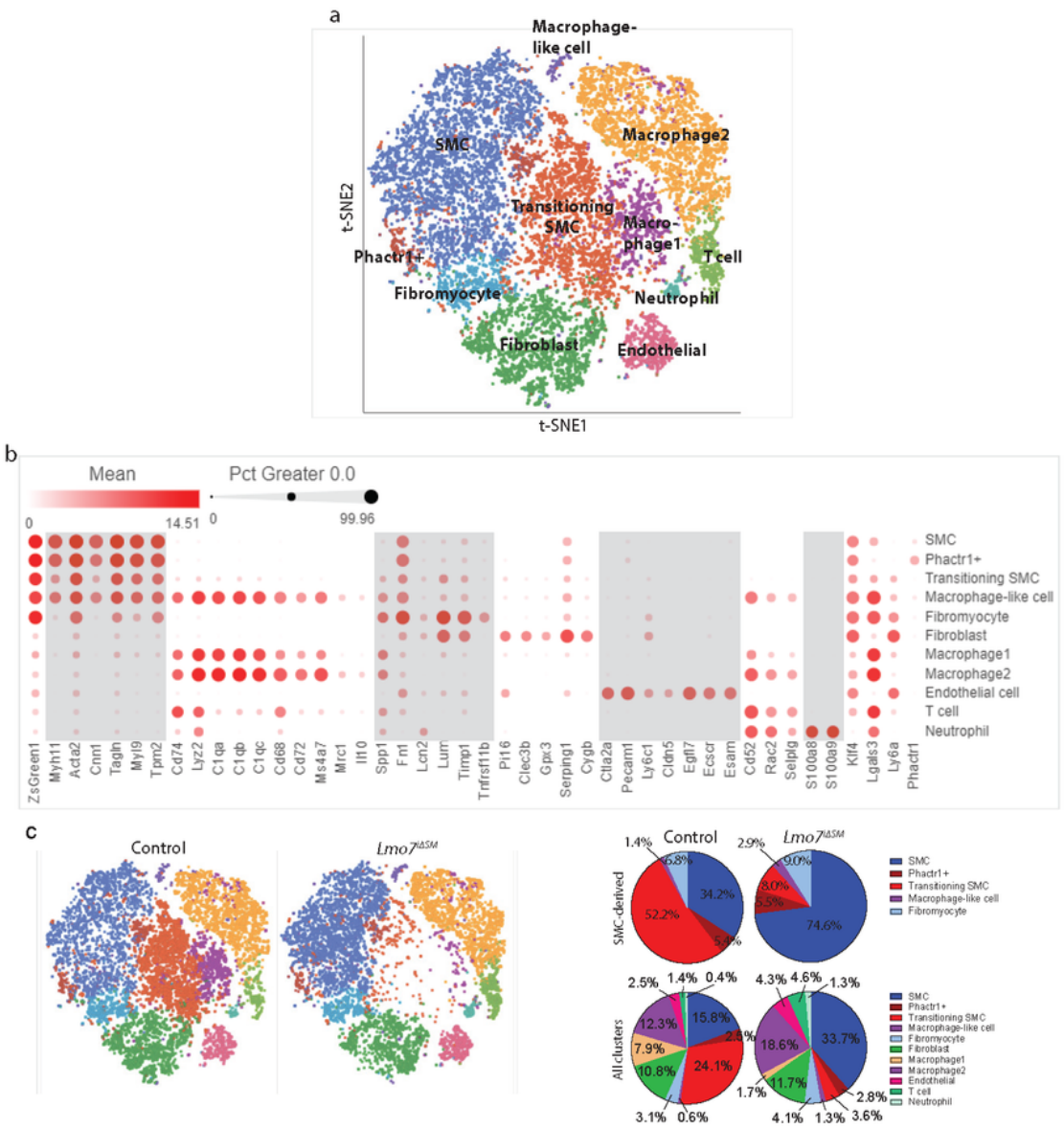

Figure 5

Single cell RNA sequencing analysis revealed distinct cell populations of SMC-derived cells in *Lmo7*$^{i\Delta SM}$ mice. (a) t-SNE visualization of cell clusters present in the atherosclerotic aortic root, aortic arch and its three main branches from control and *Lmo7*$^{i\Delta SM}$ mice combined (2 mice per genotype). (b) Heatmap visualization of marker gene expression in each cell cluster. (c) t-SNE visualization of control and

Lmo7$^{i\Delta SM}$ group separately. Pie charts show the proportion of each cluster within SMC-derived population or all the harvested cells.

Figure 6 LMO7 is induced in human atherosclerosis

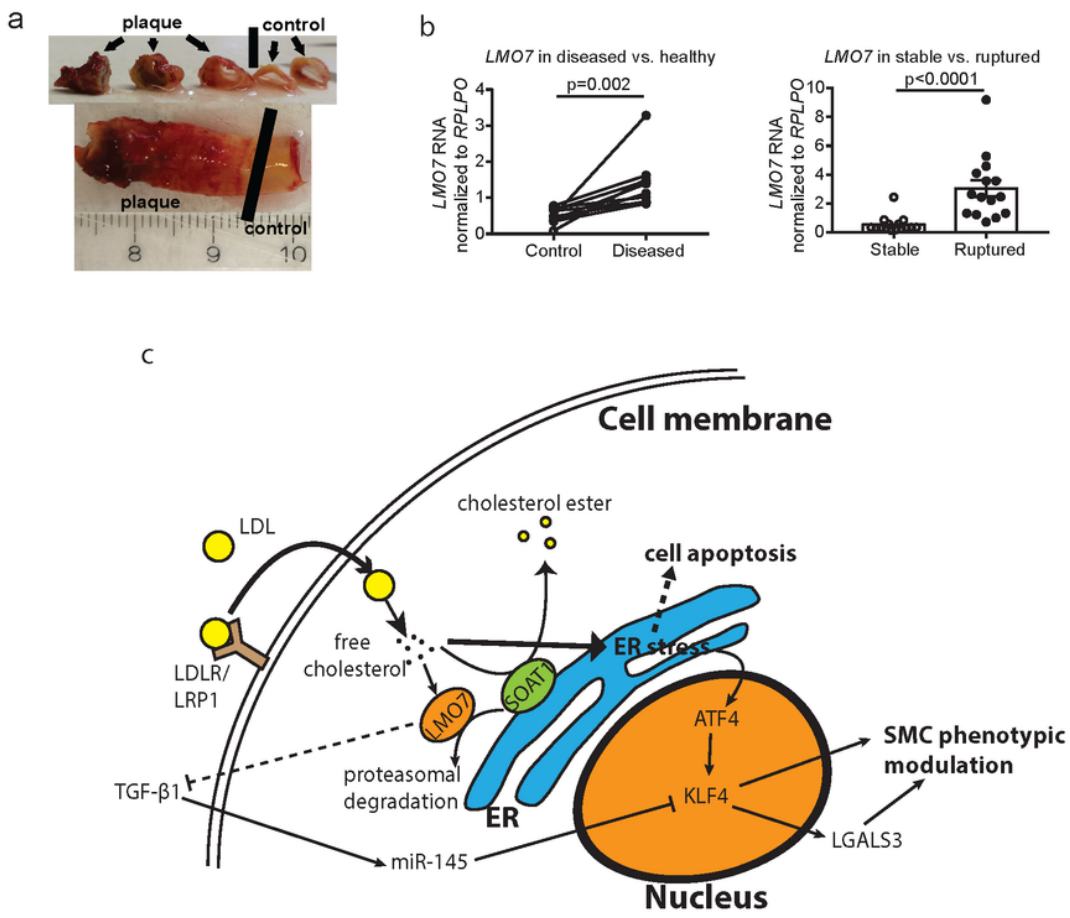

Figure 6

LMO7 RNA is induced in human atherosclerosis. (a) The diseased and non-diseased portion of human atherosclerotic carotid arteries were separated and subjected to qPCR analysis for *LMO7* (n=10). (b) The human stable atherosclerotic carotid arteries and ruptured ones were analyzed for *LMO7* RNA (n=15 for each group). (c) Schematic illustrating how cholesterol-induced LMO7 modulates SMC phenotypic modulation via regulating SOAT1 protein stability, cholesterol esterification, ER stress and KLF4/LGALS3 expression.

Supplementary Files

This is a list of supplementary files associated with this preprint. Click to download.

- SupplementaryInformatoin.docx